

Tracking kinesin-driven movements with nanometre-scale precision

Jeff Gelles*, Bruce J. Schnapp† & Michael P. Sheetz*

* Department of Cell Biology and Physiology, Washington University School of Medicine, Box 8101, 660 South Euclid Ave, St Louis, Missouri 63110, USA

† Laboratory of Neurobiology, National Institute of Neurological and Communicative Disorders and Stroke, National Institutes of Health at the Marine Biological Laboratory, Woods Hole, Massachusetts 02543, USA

Several enzyme complexes drive cellular movements by coupling free energy-liberating chemical reactions to the production of mechanical work^{1–3}. A key goal in the study of these systems is to characterize at the molecular level mechanical events associated with individual reaction steps in the catalytic cycles of single enzyme molecules. Ideally, one would like to measure movements driven by single (or a few) enzyme molecules with sufficient temporal resolution and spatial precision that these events can be directly observed. Kinesin, a force-generating ATPase involved in microtubule-based intracellular organelle transport^{4–10}, will drive the unidirectional movement of microscopic plastic beads along microtubules *in vitro*^{4,9}. Under certain conditions, a few (≤ 10) kinesin molecules may be sufficient to drive either bead movement or organelle transport. Here we describe a method for determining precise positional information from light-microscope images. The method is applied to measure kinesin-driven bead movements *in vitro* with a precision of 1–2 nm. Our measurements reveal basic mechanical features of kinesin-driven movements along the microtubule lattice, and place significant constraints on possible molecular mechanisms of movement.

Fig. 1 Stages in the high-precision measurement of relative bead position in a video frame. *a*, Image; *b*, kernel; *c*, cross-correlation of image and kernel; *d*, centroid calculation. The illustrated sequence of computations derives positional information from the entire bead image rather than from an individual point or edge only, and thereby maximizes the precision of the measurement. *a*, A segment of a digitized video frame containing the

video-enhanced DIC microscope image of a bead. The DIC image of a single bead consists of apposed bright and dark areas. The segment consists of a 49×63 rectangular matrix of integers, $I(x, y)$, each of which represents the recorded light intensity at the point (x, y) in the image (x and y are integers). *b*, A 'kernel' segment $K(x, y)$, consisting entirely of a single bead image. The centre of this segment is taken to be the point $(0, 0)$. The kernel is used as a template or standard; the effect of the calculations below is to find the position in the frame segment shown in *a* for which the surrounding intensity distribution most closely matches that surrounding the centre of the kernel. When a sequence of consecutive video frames is analysed, a single kernel derived from one of the frames is used in the analysis of all of them. The x and y dimensions of the kernel are denoted α and β , respectively; for the case shown here, $\alpha = 27$ pixels and $\beta = 33$ pixels. *c*, Cross-correlation $C(x, y)$ of the frame segment *a* with a scaled version of the kernel *b*. The cross-correlation calculation

$$C(x, y) = \sum_{i=-\alpha/2}^{\alpha/2} \sum_{j=-\beta/2}^{\beta/2} I(x+i, y+j) \{K(i, j) - s\}$$

yields sharp peaks in regions where the intensity distribution in the frame segment closely matches that in the kernel^{32,33}. The scale term s is set to the mean intensity of the pixels in the kernel. *d*, Calculation of the centroid of the peak in the cross-correlation *c*. A threshold value T is subtracted from each point in the cross-correlation and points where the difference is negative are discarded; the figure shows the 219 remaining points. From these points the coordinates of the centroid (x_c, y_c) are computed

$$x_c = \frac{\sum x \{C(x, y) - T\}}{\sum \{C(x, y) - T\}} \quad y_c = \frac{\sum y \{C(x, y) - T\}}{\sum \{C(x, y) - T\}}$$

The point (x_c, y_c) is taken as the position of the bead in *a*. In a time sequence of frame segments like *a*, the set of calculated coordinates (x_c, y_c) accurately reflect the translational movements of the bead image providing that this image (and the peak in *d*) do not significantly change shape. The absence of such a shape change was verified for all reported data. (The z -axis scale in *c* and *d* is different from that in *a* and *b*.)

Analysis of the mechanisms of force-generating enzymes such as actomyosin, dynein and kinesin has been facilitated by the development of systems in which movement can be measured *in vitro* under controlled conditions^{4,11–13}. In the experimental system for kinesin^{4,12}, a suspension of plastic beads with kinesin nonspecifically adsorbed to their surfaces is applied to purified, taxol-stabilized microtubules adhering to a glass coverslip in a buffer solution containing ATP. Video-enhanced differential interference contrast (DIC) microscopy^{14,15} is used to observe the kinesin-coated beads attach to and move along the microtubules. The plastic beads used in this assay are smaller than the resolution limit of the optical microscope and therefore produce very low-contrast images. Our technique, designed to maximize the amount of positional information extracted from low-contrast images, measures bead position in individual video frames with a precision of 1–2 nm. Similar precision has been obtained previously in light-microscope position measurements of high-contrast images (for example, ref. 16). We recorded 30 images (frames) per second on a video-disk recorder, and analysed them to determine the x and y coordinates of the beads in each frame (Fig. 1).

To determine the precision of our technique, we recorded a video sequence of stationary beads immobilized on a glass coverslip. The measured positions of two beads in this test specimen, both taken from the same sequence of video frames, are plotted in Fig. 2a, b. In both cases, the points fall in a region of width ~ 34 nm and height ~ 6 nm and display a gradual positional drift with time during the period of the measurement. The direction and magnitude of the drift are the same in Fig. 2a and b, as is the overall shape of the spatial distribution of the data points. Such drift might be caused by small movements of the specimen relative to the microscope optics. To cancel its effect on the measured positions, we used one of the stationary beads as a fiducial reference point in the specimen and measured

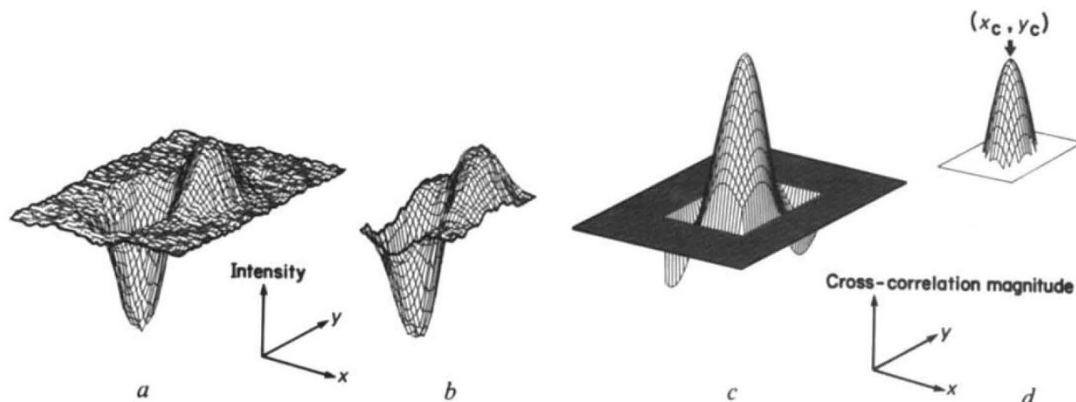
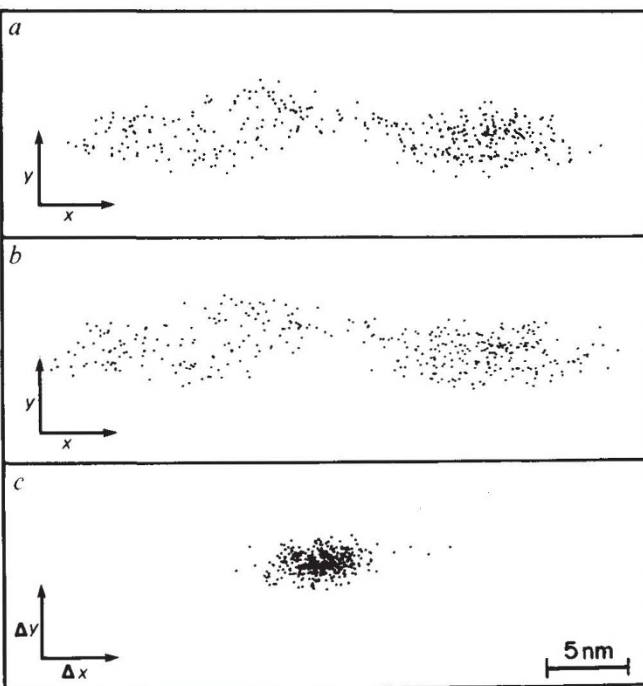


Fig. 2 The precision of the bead position measurements determined by analyses on immobilized beads. *a*, *b*, The positions measured for each of two beads in a sequence of 390 video frames (at 30 frames per second). For both the bead in *a* and that in *b*, the position data display a drift from the right to the left with time. *c*, The frame-by-frame difference of the bead coordinates shown in *a* and *b*. The *x* coordinate of each point is the *x* coordinate of a position measurement in *a* minus the *x* coordinate of the position measurement in *b* from the same video frame. The same is true of the *y* coordinates. Scale bar, 5 nm. **Methods.** 190-nm diameter carboxylated latex beads (Polysciences Inc.) adhering to a glass coverslip were surrounded by a transparent polyacrylamide gel (10% w/v) to minimize vibrational Brownian motion. The video-microscope camera output was recorded by a monochrome high-resolution optical memory disk recorder (OMDR, Panasonic TQ-2025F) at standard video-frame rates (30 frames per second). Although a frame is collected every 1/30 s, the effective temporal resolution is lower because of lag in the camera tube and because interlaced video frames partially overlap in time³⁴. The horizontal resolution of the recording is ~450 television lines per picture height. Recorded video frames were displayed by the OMDR under computer control. The video signal was processed by a 2-line time-base corrector (Fortel CCD 2h-3, 455 pixels horizontal resolution) and digitized (8-bit grey scale, 512 horizontal \times 480 vertical resolution) by a video-image processing computer (Hannaway) controlled by custom software. Sixteen independently digitized images of each frame were averaged to suppress OMDR playback noise. A rectangular subregion containing the bead image to be analysed was extracted from each digitized frame and stored in the computer system for subsequent determination of the bead coordinates. A kernel subregion restricted to the bead image was also extracted from a single (arbitrarily selected) frame of the recording. The position analysis calculation was performed on a VAX 11/785 computer (Digital Equipment). For image and kernel sizes of 62 \times 64 and 27 \times 31 pixels, respectively, the calculation required 30 s of CPU time per frame. The threshold intensity *T* was selected empirically to minimize the noise; the same value of *T* was used to analyse each frame in a given experiment. In a typical recording, 2–5% of the frames contain recording drop-outs or video-synchronization defects which distort the bead image; these frames were excluded from subsequent analyses. Magnification was calibrated against the 0.62-μm frustule spacing in the diatom *Pleurasigma angulatum*. Pixel spacing, 54 nm horizontal \times 42 nm vertical. Monte Carlo analysis of the digital centroid calculation (Fig. 1*d*) shows that the r.m.s. error introduced by digitization at this spacing is <0.5 nm.



the position of the other bead relative to it (Fig. 2*c*). The standard deviations of the positions computed in this way are 1.6 nm and 0.7 nm for the *x* and *y* coordinates, respectively, suggesting that a precision of relative bead position measurements of 1–2 nm or better can be obtained with this technique.

We examined kinesin-driven bead movements over a range of ATP concentrations (2.5 μM–1 mM). Mean bead velocities increase with increasing ATP concentration, as previously reported for kinesin-driven movements of microtubules over glass surfaces^{7,17}. A bead track from a specimen with 10 μM ATP is shown in Fig. 3*a*. The data in this figure are derived from a 16.9-s-long video recording; during this period the kinesin-coated bead moved 278 nm along a nearly vertically oriented microtubule.

Figure 3*b,c* shows the temporal relationship of the 477 individual position measurements displayed in Fig. 3*a*. Figure 3*b* shows the progress of the bead along the microtubule as measured by the projection of the bead position along the microtubule axis; Fig. 3*c* shows the small side-to-side movements perpendicular to that axis.

In Fig. 3*b* and *c*, the random scatter of the position measurements is low; it approaches that observed in the measurements on stationary beads. In contrast, the random Brownian motions of unattached beads are large even when observed with the limited temporal resolution of video measurements. The root-mean-square (r.m.s.) instantaneous velocity in the perpendicular direction is 42 nm s⁻¹ for the data of Fig. 3*c*. This is >50 times slower than the expected one-dimensional r.m.s. velocity of an unattached bead of the same size observed at 30 Hz (2.3 \times 10³ nm s⁻¹)¹⁸. The kinesin crossbridges that attach the bead to the microtubule must therefore be sufficiently short and/or rigid strongly to constrain thermally induced bead movements.

We measure the velocity of kinesin-driven bead movements along the microtubule with a much higher temporal resolution than that used previously⁴. In contrast to the uniform bead

velocities previously observed, we find that the velocity typically remains constant for an interval of only 0.1 to 2 s and then abruptly changes to a different velocity (see Fig. 3*b*, L and H), ranging from more than twice the overall mean velocity down to zero. Such variations were observed at all ATP concentrations from 10 to 1,000 μM. They could be caused by local inhomogeneities in microtubule structure, by fluctuations in the number of active force generators (compare refs 19 and 20), or by other factors. Many recordings also contained negative velocity intervals during which the bead moved backwards (usually by not more than 10 nm).

When no ATP is present, kinesin-coated beads attach to the microtubules and do not move⁴. At millimolar ATP concentrations, beads move at a maximal rate (under the assay conditions of Vale *et al.*⁹) of 500–600 nm s⁻¹. For an object moving at this velocity, the fundamental mechanical processes that produce movements (which are assumed to have a nanometre size scale) will have a frequency too high to be resolved by our instrumentation; however, we can slow such processes to an observable rate by reducing the ATP concentration.

Figure 4 shows the movement along the microtubule axis of a kinesin-coated bead in the presence of 2.5 μM ATP; its mean velocity is less than 1% of maximal. Unlike those moving at higher speeds (compare with Fig. 3), beads in this very low-velocity regime show two distinct types of motion. During some periods, movement occurs smoothly with low instantaneous velocities (see Fig. 4, region A). During other periods, however, the bead remains stationary most of the time and moves forward in sudden jumps (see Fig. 4, region B). The jump duration is usually less than two frame times (67 ms), and most jumps are ~4 nm in length. The distribution of observed data-point separation distances (not shown) confirms the tendency of the beads to stop at positions separated by ~4 nm or integer multiples of that value. This regularity might be caused by features of the kinesin mechanochemical cycle in which microtubule binding

Fig. 3 Motion of a kinesin-coated bead along a microtubule in the presence of $10 \mu\text{M}$ ATP. *a*, The bead track, consisting of bead-position measurements at 30 Hz. Scale bar, 50 nm. *b*, The projection of the bead position along the direction of the bead track as a function of time. For the entire record the mean velocity is 16.1 nm s^{-1} ($\sim 3\%$ of the maximal velocity). L and H, two segments with mean velocities of 8.2 and 36.2 nm s^{-1} , respectively. *c*, The projection of the bead position along the direction perpendicular to the bead track as a function of time.

Methods. Kinesin was purified from squid optic lobes using a monoclonal antibody⁹ against the 110K polypeptide^{17,35}. We observed the motion of kinesin-coated beads on taxol-stabilized microtubules adsorbed to a coverslip silanized with dichlorooctamethyl-tetrasiloxane (Surfasil, Pierce), which made up one wall of a laminar flow chamber³⁶.

Silanizing the glass minimizes the attachment of kinesin and the resultant 'gliding' of microtubules on the glass surface⁴. We added $10 \mu\text{l}$ of 2.5% (w/v) 150-nm diametre carboxylated latex beads to $90 \mu\text{l}$ kinesin in PEM buffer⁴ supplemented with $10 \mu\text{M}$ ATP, 80 mM KCl and 0.02% Triton X-100 to give a final kinesin 110K subunit concentration of 80 nM . This suspension of kinesin-coated beads was then introduced into the flow chamber and observed with a video-enhanced differential interference contrast imaging system consisting of a Zeiss ICM inverted microscope and a Dage-MTI 68 series Newvicon video camera. This system is described in detail elsewhere³⁷, with the exception of a new illuminator incorporating a fibre-optic scrambler^{34,38}. The illuminator focuses a 100-W mercury arc lamp (filtered with IR and UV absorbing filters and an interference filter with a 50-nm half width centred at 550 nm) onto a 0.75-nm diameter plastic optical fibre. The output of the fibre, which serves as a point illumination source for the microscope optics, was collected with a Zeiss infinity-corrected Neofluar objective and projected with a two-element achromat onto the condenser aperture. The focal length of the achromat was chosen to fill the aperture with an image of the fibre tip. Glan-Thompson prisms replaced the film polarizer and analyser supplied with the Zeiss DIC optics. These modifications provide significantly brighter and more even illumination, and allow higher magnification in the projection of the microscope image onto the video camera target. Video frames were recorded, digitized and processed as described in Figs 1 and 2. The *x* and *y* coordinates are the frame-by-frame differences between those of the moving bead and those of a stationary reference bead in the same frame, as in Fig. 2c. The microtubule orientation used in calculating (*b*) and (*c*) was determined by a linear least-squares fit to the points in *a*. Pixel size, 22 nm horizontal \times 17 nm vertical.

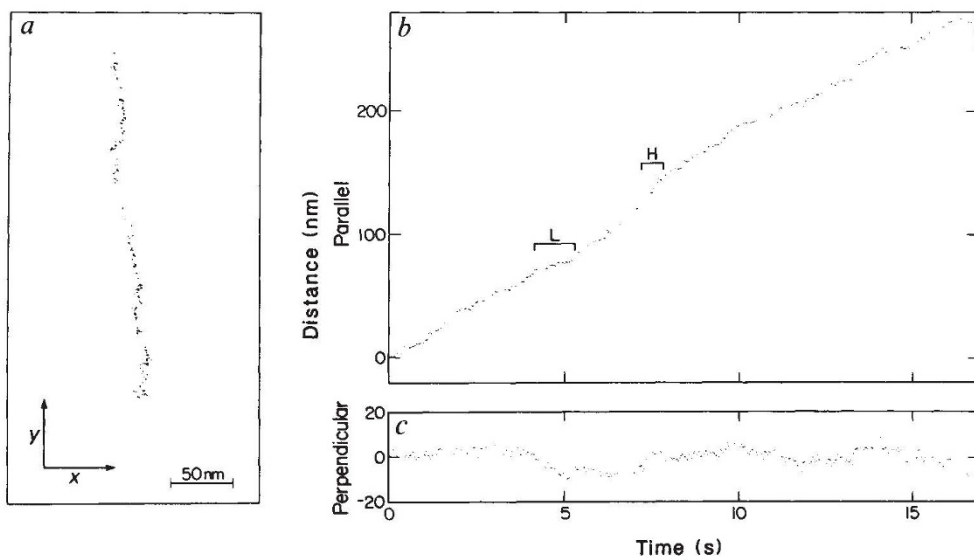
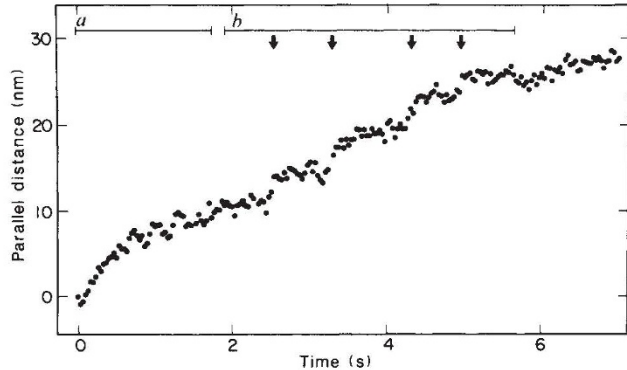


Fig. 4 Motion of a kinesin-coated bead along a microtubule in the presence of $2.5 \mu\text{M}$ ATP. The plot shows the projection of the bead position along the microtubule axis as a function of time. The mean velocity along the microtubule axis over the period shown is 3.9 nm s^{-1} ($\sim 0.8\%$ of maximal velocity). Forward movement in region A occurs smoothly with a mean velocity of 5.6 nm s^{-1} . Movement in region B occurs in four discrete jumps (arrows) of length $3.7 \pm 1.7 \text{ nm}$ (mean \pm s.d.).

Methods. The sample was identical to that of Fig. 3, except for a lower ATP concentration ($2.5 \mu\text{M}$). The data-analysis procedure was identical to that of Fig. 3 except that microtubule orientation was determined manually from the positions of video cursors superimposed on the centre of the microtubule image at distances of $0.5 \mu\text{m}$ on either side of the microtubule segment on which the bead motion occurred.



sites on kinesin interact specifically with a domain on periodically spaced tubulin monomers (spacing, 4 nm).

Because of the symmetry of the microtubule lattice (refs 21, 22, but see ref. 23), it is likely that identical sites for the binding of kinesin are distributed around the entire circumference of the microtubule. Despite the presence of closely spaced repeating structures over the entire microtubule surface, we do not observe any tendency for the beads to 'wander' circumferentially on the surface as they move axially over hundreds of nanometres (Fig. 3c). The absence of substantial lateral movement is intriguing when one considers the geometry of a bead attached by a kinesin crossbridge to a site on a microtubule protofilament: if the crossbridge moves from one site to a second site on an adjacent protofilament, the expected displacement of the bead centre would be between 40 and 56 nm (assuming a crossbridge length of $\sim 30 \text{ nm}$ ²⁴⁻²⁶). The observed movements rarely

exceed half of these amounts (see Fig. 3c), which suggests that the bead maintains a position above a particular protofilament (or above the junction between the members of a particular protofilament pair) as it moves axially. In experiments in which several beads moved over the same segment of a microtubule, the beads followed different paths, all approximately parallel, at lateral positions over a region up to 130 nm wide. This observation may help to explain how organelles moving on microtubules pass one another without apparent collision²⁷⁻³⁰.

The simplest explanation for the restriction of lateral bead motion is that each kinesin molecule binds to sites associated with a particular protofilament (or set of adjacent protofilaments) as the bead moves along the microtubule. If a bead is attached to the microtubule with several kinesin molecules, the shift of a single molecule from one protofilament to another might produce only an insubstantial change in the circumfer-

tial position of the bead. However, both structural and energetic considerations^{4,5,11,24–26,31} suggest that the number of kinesin crossbridges linking the bead and the microtubule is small, so that even the fluctuations in the average circumferential position taken over all the crossbridges would be substantial if each crossbridge had no tendency to maintain its association with a particular protofilament.

The methods used here could be used to explore various aspects of kinesin-based movement, including characterization of the force-generating step in the mechanochemical cycle and analysis of the mechanical properties of bead attachment to microtubules in different states of the enzyme. More generally, the ability to measure molecular-scale movements of small objects in real time in the light microscope has potential for providing insights into various cellular processes.

We thank Stephen G. Turney for assistance with the instrumentation and computer software and Thomas S. Reese for his support. We also thank Wyndham Hannaway, Elliot Elson, Hong Qian and Shahid Khan for discussions. Dr Matthew Suffness (NCI) provided the taxol. Supported in part by grants from the National Institutes of Health (to M.P.S.) and a Damon Runyon-Walter Winchell Cancer Fund Fellowship (J.G.).

Received 16 October; accepted 16 December 1987.

1. Eisenberg, E. *Lect. Math. Life Sci.* **16**, 19–59 (1986).
2. Berg, H. C. & Khan, S. in *Mobility and Recognition in Cell Biology* (eds Sund, H. & Veeger, C.) 485–497 (de Gruyter, Berlin, 1983).
3. Johnson, K. A. A. *Rev. Biophys. biophys. Chem.* **14**, 161–188 (1985).

Protein-disulphide isomerase and prolyl isomerase act differently and independently as catalysts of protein folding

Kurt Lang & Franz X. Schmid

Institut für Biophysik und Physikalische Biochemie,
Universität Regensburg, D-8400 Regensburg, FRG

Two enzymes are now known that catalyse slow steps in protein folding. Peptidyl-prolyl *cis-trans* isomerase¹ catalyses the *cis-trans* isomerization of Xaa-Pro peptide bonds in oligopeptides and during the refolding of several proteins^{2,3}. The other enzyme, protein-disulphide isomerase, accelerates the reactivation of reduced proteins, presumably by catalysis of thiol-disulphide exchange reactions^{4–6}. Recent evidence indicates that the β -subunit of prolyl 4-hydroxylase, an enzyme involved in collagen biosynthesis, is identical with disulphide isomerase^{7,8}. On the basis of this important finding, it was suggested⁹ that disulphide isomerase accelerates protein folding, not by ‘reshuffling’ incorrect disulphide bonds, but in the same way as prolyl isomerase by catalysing proline isomerization which is known to be important for the folding of collagen¹⁰ and other proteins. Here we show that the catalytic activities of these two enzymes are different. Disulphide isomerase accelerates the reformation of native disulphide bonds during protein reoxidation. We find no evidence that this enzyme can catalyse the isomerization of proline peptide bonds, a reaction efficiently accelerated by prolyl isomerase. When both enzymes are present simultaneously during protein folding, they act independently of one another.

Prolyl isomerase activity is measured in a coupled assay with chymotrypsin, using the short oligopeptide *N*-succinyl-Ala-Ala-Pro-Phe-*p*-nitroanilide¹. The *p*-nitroanilide moiety can only be cleaved off rapidly by chymotrypsin when the preceding Ala-Pro peptide bond is in the *trans* conformation. At equilibrium about 10% of the peptide has a *cis* Ala-Pro bond. In the presence of a high protease concentration, hydrolysis of the *trans* peptide

4. Vale, R. D., Reese, T. S. & Sheetz, M. P. *Cell* **42**, 39–50 (1985).
5. Kuznetsov, S. A. & Gelfand, V. I. *Proc. natn. Acad. Sci. U.S.A.* **83**, 8330–8334 (1986).
6. Cohn, S. A., Ingold, A. L. & Scholey, J. M. *Nature* **328**, 160–163 (1987).
7. Porter, M. E. et al. *J. biol. Chem.* **262**, 2794–2802 (1987).
8. Khan, S., Schnapp, B. J. & Sheetz, M. P. *Biophys. J.* **49**, 415a (1986).
9. Vale, R. D. et al. *Cell* **43**, 623–632 (1985).
10. Schroer, T. A., Schnapp, B. J., Reese, T. F. & Sheetz, M. P. (in preparation).
11. Sheetz, M. P. & Spudich, J. A. *Nature* **303**, 31–35 (1983).
12. Vale, R. D., Schnapp, B. J., Reese, T. S. & Sheetz, M. P. *Cell* **40**, 559–569 (1985).
13. Vale, R. D. & Toyoshima, Y. Y. *J. Cell Biol.* **105**, 96a (1987).
14. Allen, R. D., Allen, N. S. & Travis, J. L. *Cell Motil.* **1**, 291–302 (1981).
15. Allen, R. D. *A Rev. Biophys. biophys. Chem.* **14**, 265–290 (1985).
16. Howard, J. & Hudspeth, A. J. *Proc. natn. Acad. Sci. U.S.A.* **84**, 3064–3068 (1987).
17. Schnapp, B. J., Chrise, B. J., Khan, S., Sheetz, M. P. & Reese, T. F. *Nature* (submitted).
18. MacDonald, D. K. C. *Noise and Fluctuations: An Introduction* (Wiley, New York, 1962).
19. Block, S. M. & Berg, H. C. *Nature* **309**, 470–472 (1984).
20. Khan, S., Meister, M. & Berg, H. C. *J. molec. Biol.* **184**, 645–656 (1985).
21. Amos, L. A. in *Microtubules* (eds Roberts, K. & Hyams, J. S.) 1–64 (Academic, London, 1979).
22. Mandelkow, E.-M. & Mandelkow, E. *J. molec. Biol.* **181**, 123–135 (1985).
23. Mandelkow, E.-M., Schultheiss, R., Rapp, R., Müller, M. & Mandelkow, E. *J. Cell Biol.* **102**, 1067–1073 (1986).
24. Miller, R. H. & Lasek, R. J. *J. Cell Biol.* **101**, 2181–2193 (1985).
25. Gilbert, S. P., Allen, R. D. & Slobooda, R. D. *Nature* **315**, 245–248 (1985).
26. Amos, L. A. *J. Cell Sci.* **87**, 105–111 (1987).
27. Koonce, M. P. & Schliwa, M. J. *J. Cell Biol.* **100**, 322–326 (1985).
28. Schnapp, B. J., Vale, R. D., Sheetz, M. P. & Reese, T. S. *Cell* **40**, 455–462 (1985).
29. Allen, R. D. et al. *J. Cell Biol.* **100**, 1736–1752 (1985).
30. Hayden, J. H. & Allen, R. D. *J. Cell Biol.* **99**, 1785–1793 (1984).
31. Langford, G. M., Allen, R. D. & Weiss, D. G. *Cell Motil. Cytoskel.* **7**, 20–30 (1987).
32. Ballard, D. H. & Brown, C. M. *Computer Vision* (Prentice-Hall, Englewood Cliffs, New Jersey, 1982).
33. Gonzalez, R. C. & Wintz, P. *Digital Image Processing* (Addison-Wesley, Reading, Massachusetts, 1977).
34. Inoué, S. *Video Microscopy* (Plenum, New York, 1986).
35. Steuer, E., Vale, R. D., Schnapp, B. J., Reese, T. S. & Sheetz, M. P. *J. Cell Biol.* **101**, 397a (1985).
36. Berg, H. C. & Block, S. M. *J. gen. Microbiol.* **130**, 2915–2920 (1984).
37. Schnapp, B. J. *Meth. Enzym.* **134**, 561–573 (1986).
38. Ellis, G. W. *J. Cell Biol.* **101**, 83a (1985).

occurs within a few seconds. Cleavage of the *cis* peptide, however, is limited in rate by the *cis* to *trans* isomerization of the Ala-Pro bond, which shows a time constant of 115 s at 10 °C. This reaction is efficiently catalysed by prolyl isomerase (Fig. 1a), whereas disulphide isomerase does not affect the rate of this isomerization either in the absence (Fig. 1b) or in the presence of prolyl isomerase (Fig. 1c). So under conditions where prolyl isomerase is a good catalyst, disulphide isomerase has no effect on the isomerization of the Ala-Pro bond in the test peptide.

In addition to being inactive as a prolyl isomerase when assayed with a short peptide, disulphide isomerase is unable to accelerate the slow refolding of a protein with intact disulphide bonds, such as the immunoglobulin light chain from mouse. It has been suggested that this reaction involves proline isomerization¹¹, and recently it was found to be accelerated by prolyl isomerase³. Figure 2a shows the catalysis of the slow refolding of this protein by prolyl isomerase. Under the same conditions, addition of disulphide isomerase at two different concentrations had no influence on the refolding of the immunoglobulin light chain (Fig. 2b). Also, disulphide isomerase did not affect the accelerated reaction when the concentration of disulphide isomerase was varied during refolding in the presence of 0.21 μ M prolyl isomerase (Fig. 2c).

Disulphide isomerase catalyses the reactivation of reduced and unfolded proteins^{4–6,12}. Figure 3 shows the acceleration of the reactivation kinetics of reduced ribonuclease A (RNase A) by disulphide isomerase. The reactivation experiments were performed in the presence of a mixture of reduced (4 mM) and oxidized glutathione (0.4 mM) at pH 7.8 and 25 °C. These are conditions where RNase A can be reactivated in the absence of disulphide isomerase, and where prolyl isomerase shows high activity towards proline-containing substrates. Addition of prolyl isomerase in variable amounts to the reoxidation mixture had no influence on the rate of reactivation of reduced RNase A (Fig. 3). In experiments where both disulphide isomerase and prolyl isomerase enzymes were present simultaneously, only a variation of the disulphide isomerase concentration affected the rate of reactivation (Fig. 3). The experiments shown in Figs 2c and 3 are complementary: they show that the two enzymes act